UM NM 73-1

Coded Aperture Gamma-Ray Imaging with Stochastic Apertures

A. Z. AKCASU*
R. S. MAY*
G. F. KNOLL*
W. L. ROGERS**
K. F. KORAL**
L. W. JONES***

November 1973

Text of talk delivered at Society of Photo-Optical Instrumentation Engineers Seminar on Application of Optical Instrumentation in Medicine. November 29, 30, 1973, Chicago, Illinois.

*Department of Nuclear Engineering
**Division of Nuclear Medicine
***Department of Physics


THE UNIVERSITY OF MICHIGAN
THE UNIVERSITY OF MICHIGAN
1817
LIBRARIES

tional approach, but the additional degree of freedom introduced by the time modulation will be seen to have important consequences.

ONE-DIMENSIONAL CODED APERTURE

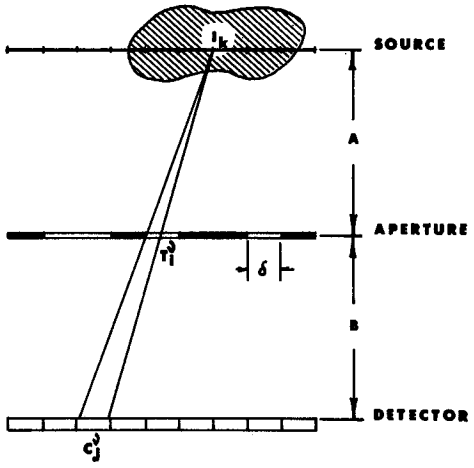

Figure 1. Geometric arrangement for a 1-dimensional coded aperture.

One now records a sequence of M coded images using the M aperture plates. Assuming that each coded image and aperture function are digitized and represented respectively by N_d and N_f numbers, the recorded data consists of:

i) $C^{\nu}{}_j$ = number of counts recorded by the jth detector element during the νth time interval. ($\nu=1,\ldots,M$; $j=1,\ldots,N_d$.)

ii) $T_i{}^{\nu}$ = transmittance (probability of photon transmission) of the ith aperture element during the νth time interval. ($\nu=1,\ldots,M$; $i=1,\ldots,N_f$.)

The object is to somehow use these recorded data to estimate the spatial source distribution, which is represented in discrete form by:

$$I_1,\ldots,I_k,\ldots,I_e \quad .$$

So far nothing has been said about the aperture functions T^{ν} . The philosophy behind the approach is most easily defined by describing the stochastic aperture.

A. Stochastic Aperture

Suppose that we generate the M aperture representations by choosing member functions of some prespecified stationary random process T , whose mean and autocovariance function are denoted by:

$$m \equiv \langle T(y) \rangle$$

and

$$\Phi(y-y') = \langle (T(y)-m)(T(y')-m) \rangle . \quad (1)$$

Each aperture can be considered to be a sample or a "realization" of the stochastic process T . We can further identify time fluctuations in transmittance by:

$$t(\nu) = T^{\nu} - m \quad . \quad (2)$$

The autocovariance function Φ of the generating process is a measure of the extent of interdependence between transmission values at various positions. Φ is a peaked function whose half width and tail properties determine respectively the resolution and side lobe properties of the point response function. Unlike fixed coded aperture techniques, the integral properties of any particular aperture function are unimportant; only collective aspects are of interest. The crucial point is that time dependent transmittances are uncorrelated for different locations on the aperture plane.

In practice the generating process T often consists of a class of piecewise constant binary functions which assume only the values of 0 and 1 .

Equation (1) can be reexpressed in discrete form as:

$$\Phi_{i,i'} = \langle (T_i-m)(T_{i'}-m) \rangle \quad . \quad (3)$$

The smallest interval, designated a filter increment, δ , directly determines the width of the function Φ . As well as facilitating aperture construction, a binary transmission func-

tion generally provides statistical properties superior to classes which allow continuous values between 0 and 1 .

B. Cross Correlation

Using the data described above, we can compute and store the following "Temporal" cross correlations between observed counts and aperture transmittance fluctuations:

$$Q_{ij} \equiv \frac{1}{M} \sum_{\nu=1}^{M} c_j^{\nu} \, (T_i^{\nu} - m) \qquad (4)$$

where $i=1,\ldots N_f$

$j=1,\ldots N_d$.

These numbers constitute an N_f by N_d matrix. $\underline{Q}$ contains all the available information from the above measurement.

It has been shown (Ref. 9,10,11) that an estimate of the source strength $\bar{I}_k$ can be specified by a linear combination of the elements Q_{ij} ; that is, there exist coefficients $\alpha^k{}_{ij}$ dependent only on the experimental geometry such that:

$$\bar{I}_k = \sum_{ij} \alpha^k{}_{ij} Q_{ij}$$

$$= \sum_{j=1}^{N_d} \sum_{i=1}^{N_f} \alpha_{ij}{}^k \frac{1}{M} \sum_{\nu=1}^{M} c^{\nu}{}_j (T_i{}^{\nu} - m) \; . \qquad (5)$$

The α's are non-zero only for those aperture elements, T_i^{ν} , which lie between the kth source element and the jth detector. Examination of Figure 1 further shows that the α's select a unique collection of aperture elements for every resolvable image point. This is true even though only a single detector element is used. (However, both statistical accuracy and depth information is gained by using many detector elements.) As M become infinite these unique collections of aperture elements become orthogonal as determined from Equation 3 and the assumed randomness of the process T . If detector resolution is not a factor, the image resolution, R, becomes:

$$R \cong \frac{A + B}{B} \, \delta \qquad (6)$$

where A and B are the source-to-aperture and aperture-to-detector distances respectively and δ is the width of the smallest filter interval.

Of more practical interest is the mean response encountered for finite M excluding the photon statistics. Figure 2 shows the point response calculated for 500 realizations of a one dimensional stochastic aperture and infinite photon statistics.

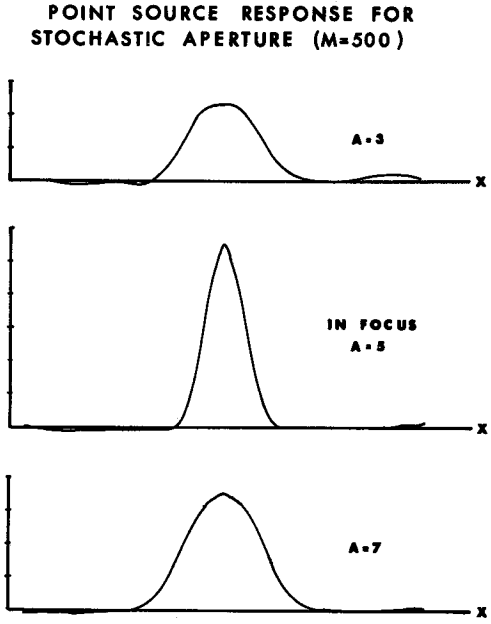

Figure 2. Point source response for 500 realizations of a stochastic aperture.

Some small sidelobes are in evidence whose average amplitude decreases roughly as $\sqrt{1/M}$. The peak width is found to be relatively insensitive to M . The peak is defocused smoothly but assymetrically in depth. More rapid defocusing occurs for planes closer to the aperture since the subtended angle changes more rapidly.

It is of paramount importance to understand the effect of photon statistics in a coded aperture imaging scheme if it is to be applied in Nuclear Medicine. The quantity of interest is the variance of the mean response function defined as

$$\langle f_M(x)^2 \rangle - \langle f_M(x) \rangle^2 \quad .$$

This will give rise to a standard deviation equal to

$$\sqrt{\text{Var } f_M(x)} \quad \text{where} \quad f_M(x) \quad \text{is}$$

the mean response. The variance at any position may be expressed as the convolution of the source distribution with an error kernel, $E_M(x - x')$. The shape of the error kernel is strongly dependent upon the mean transmission of the aperture, m . Error kernels calculated for uniform distributions and several values of m are illustrated in Figure 3.

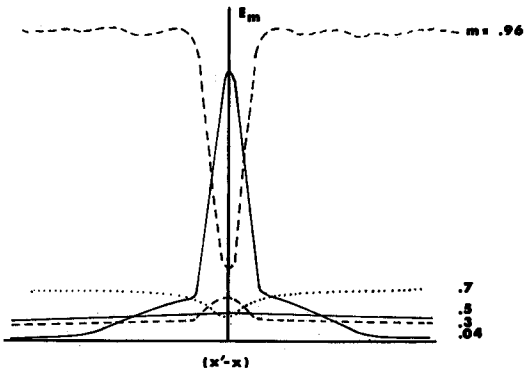

Figure 3. Plot of error kernel normalized to mean response as a function of displacement for several values of mean transmission.

For m large the error is locally small reflecting good counting statistics. The large wings show that distant sources will strongly affect the local error. For m = 0.5, the error distribution is approximately uniform indicating that all source locations contribute equally to the error and that the error is proportional to the integrated signal strength. As the mean transmission is further reduced, approaching the pinhole as a limit, the error is locally increased reflecting poor counting statistics, but the wings are reduced indicating that neighboring sources contribute significantly less to the local error. This dependence of the error on mean transmission is explicitly illustrated in Figure 4 for the case of a point source. Since the mean transmission is readily varied, a method is available for optimizing the aperture for a given source distribution.

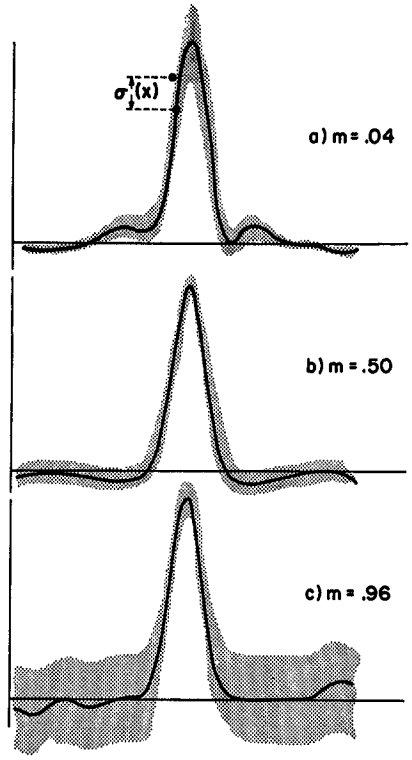

Figure 4. Illustration of the error distribution about a point source for 3 different mean transmissions.

The mean transmission need not be spatially uniform, but the effect of varying this parameter has not yet been determined.

A digital Monte Carlo simulation has been made to compare a pinhole and a stochastic aperture of mean transmission, m = 0.5 for the case of a pair of adrenal glands. They were represented by point sources in a continuous background distribution having both width and depth as shown in Figure 5.

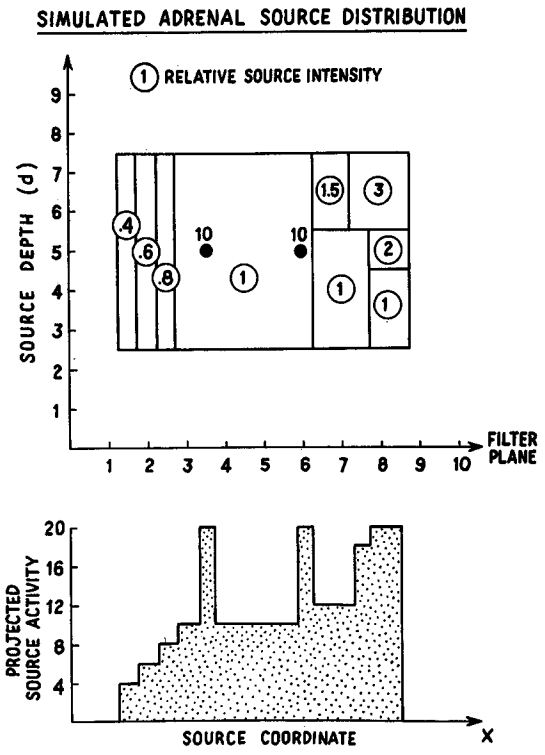

Figure 5. Source distribution used for 1 dimensional simulation of adrenal glands. The detector is 10 units wide and located 4 units below the filter or aperture plane.

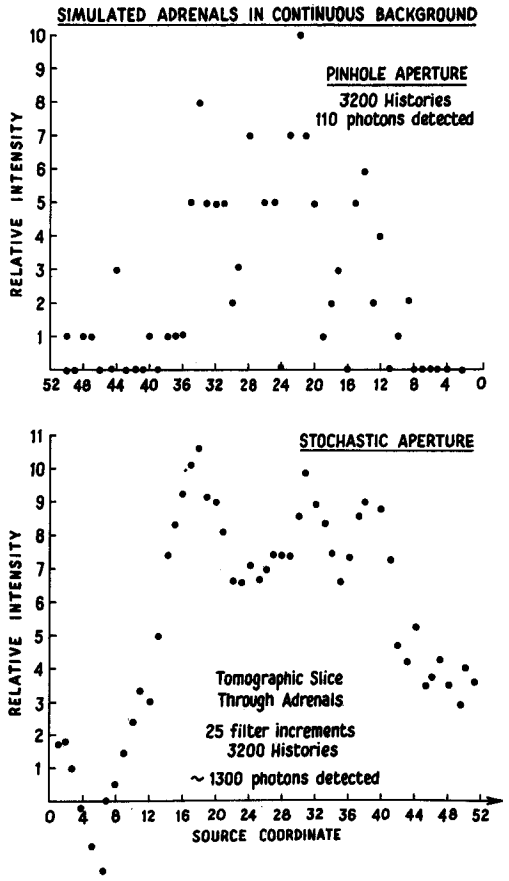

Figure 6. Reconstructed images of the adrenal using the pinhole aperture (Top) and stochastic aperture (Bottom).

The background increases to the right to simulate the liver, and the projected source distribution is typical of that observed about 8 days post-injection. The source distribution was viewed for equal time and at equal resolution by the two apertures. The pinhole image is shown at the top of Figure 6 and that from the stochastic aperture at the bottom. The calculated error in this image is uniformly distributed (see Figure 3) and equal to 1.5 relative intensity units. This gives an error in the left adrenal peak height of 13.9%. The pinhole data which must be averaged over 3 detector elements shows an error of 23.5%. In order to achieve comparable accuracy the pinhole exposure time would need to be increased a factor of 2.9. Further improvement would follow optimization of the mean transmission.

Note that an estimate based solely on the increased solid angle of the stochastic aperture would predict a factor of 12 difference in exposure times. The smooth appearance of the stochastic aperture image not only results from increased statistical accuracy but is a reflection of the fact that the statistical fluctuations have a correlation length equal to the spatial resolution. Such smoothing is optimal in the sense that it engenders no loss in spatial resolution.

C. Pseudo-Random Strings

Although it is possible to reduce the sidelobes on the point response function to an arbitrarily small value

by increasing the number of random realizations, it is reasonable to expect that for a finite number of realizations there will be a "best set" of realizations which will exhibit the orthogonal property obtained from the infinite set of random realizations. This is indeed true, and such sets have been widely employed in neutron and molecular beam time-of-flight spectroscopy (Ref. 13, 14). These sets may be generated by cyclic permutation of pseudo-random strings of 1's and 0's, such as Barker codes, which exhibit a peaked auto-covariance function with zero sidelobes. For a string length M, the collection of M cyclic permutations forms a complete, orthogonal basis set. Numerous such strings of varying length and mean transmission have been tabulated (Ref. 13, 14).

Despite the fact that these strings are one dimensional, they may be distributed over a two dimensional aperture plate. This follows from the method's dependence on the time integral rather than the spatial integral. It is important however that no two points on the plate simultaneously describe identical non-zero sequences. This would destroy the orthogonality condition between points on the aperture. A section through the center of a two-dimensional point response function obtained with a 40 element string distributed in a 6 x 6 matrix is shown in Figure 7 both in and out of focus. The 40 realizations were generated by permuting the string, one element at a time, through its full length. (The fact that 4 elements were left over makes no difference.) The result is similar to that obtained with 500 random realizations mentioned earlier except that in the present case there are no sidelobes. The slight negative bias can be eliminated by correction for the finite string length.

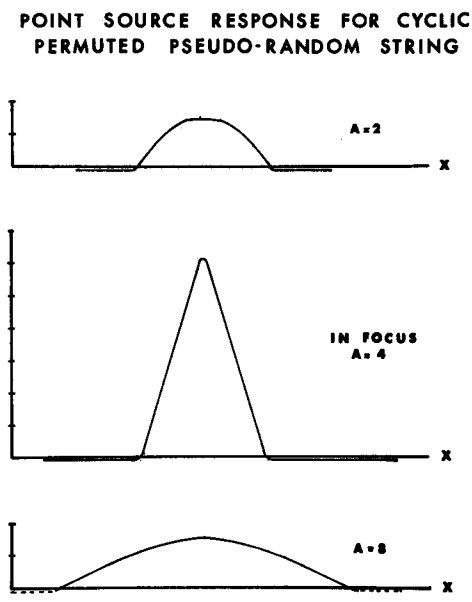

Figure 7. Point response obtained using a cyclically permuted 40 element pseudo-random string. Three focal depths are illustrated.

D. Relation to Fixed Aperture

It is perhaps of interest to explore in a qualitative way the relationship of the time modulated aperture to a fixed aperture. To do this reconsider the expression (Eq. 5) for the strength of the kth source element, I_k, and reverse the order of temporal and spatial summation:

$$I_k = \frac{1}{M} \sum_{\nu=1}^{M} \sum_{i,j} \alpha_{ij}^{k} \, C_j^{\nu} (T_i^{\nu} - m) \qquad (7)$$

From the geometric relations in Figure 1, i is given by:

$$i = \beta k + \gamma j \quad , \quad \beta = \frac{B}{A+B} \quad , \quad \gamma = \frac{A}{A+B} \; . \qquad (8)$$

with suitable allowance made for handling the discrete quantities. The sum over i and j reduces to a single sum:

$$I_k = \sum_{\nu=1}^{M} \sum_{j}^{N_d} \alpha_{(\beta k+\gamma j)} C_j^{\nu} \; (T^{\nu}_{\beta k+\gamma j} - m). \quad (9)$$

The image is now expressed in terms of a coherent summation of M scaled spatial cross correlations between the coded image and fluctuations in the mean transmission. The question which comes immediately to mind is, "Why not choose a transmission function which has a peaked spatial autocorrelation like a zone plate and just let M = 1 ?" Part of the answer lies in the manner in which the reconstructed image goes out of focus. Examples are shown in Figures 8 and 9. Figure 8 illustrates the case for one of the pseudo-random strings which, as we previously indicated, does have a peaked auto correlation. The point response which is sharply peaked without sidelobes for the in-focus case deteriorates seriously as it goes out of focus. When M such correlations are summed for the permuted string, however,the spurious oscillations add to zero and the result shown previously in Figure 7 is obtained.

The second example, Figure 9, is for an on-axis zone plate. The letters K and R were in planes separated by 3 cm. With the R in focus the K has degenerated into 4 individual K's. Off-axis zone plates do not demonstrate quite such a dramatic effect, but do, never-the-less cause problems for out of focus sources.

Imaging with stationary codes and by temporal modulation differ fundamentally from each other in the operations and conditions necessary for their success. The stationary code relies upon a spatial integration to provide the completeness relationship which guarantees a peaked response function free of spurious structure; this relationship breaks down when the scale of a code is varied (as for sources at different depths) or when the integration cannot be completed (such as when a portion of the aperture shadow falls beyond the detector boundary).

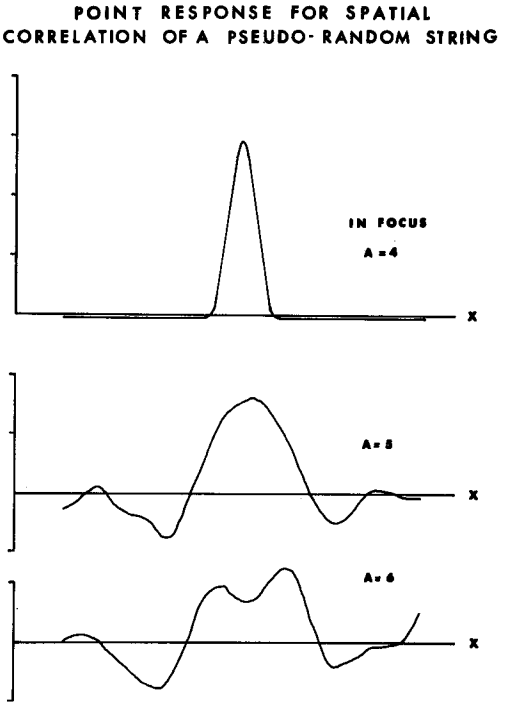

Figure 8. Point response obtained using spatial correlation of a pseudo-random string. Three focal depths are illustrated.

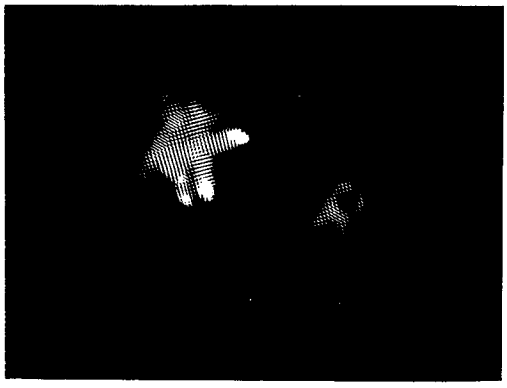

Figure 9. Illustration of out-of-focus behavior of on-axis zone plate. The defocussed letter breaks into 4 components corresponding to the 4 orders of the half-tone screen.

In contrast, a time modulated aperture requires only that the time fluctuations in transmittance are uncorrelated for any two points in the aperture plane separated by more than a filter increment. A point-by-point reconstruction is thus obtained which allows us to produce a good response function based upon even a single detector element. Depth information and improved statistical accuracy may be gained by combining results from many elements, but the important point is that no spatial integration is necessary so that questions of scale and integration limits do not even arise.

III. Experimental Implementation

We have constructed a time modulated aperture plate based on a 121 element pseudo-random string. The string has 40 open elements for a mean transmission of 33%. The filter increment of 3 mm was selected for use on an Anger camera. A photograph of the aperture is shown in Figure 10. The code is arranged on the plate so that advancing the plate by one filter increment permutes the string cyclically by one step for each of the 121 filter elements being viewed by the detector. The detector view is limited by a 3.3 cm square aperture beneath the code plate.

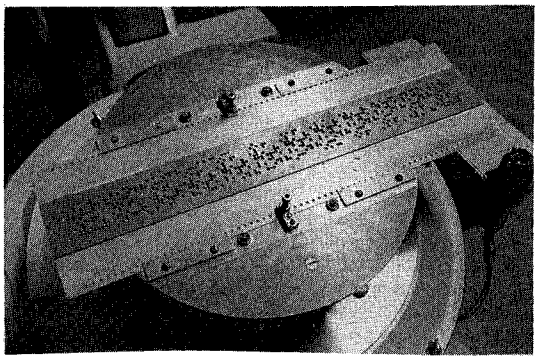

Figure 10. Photograph of coded lead aperture. The code is based on a 121 element pseudo-random string. Each aperture realization is accomplished by moving the plate one filter increment. The 11 x 11 aperture area is defined by a 3.3 cm square aperture beneath the code plate.

Data is acquired using a Medical Data Systems computer system based on a Data General NOVA computer with dual disks. The 121 short exposures are sequentially recorded on one of the disks for reconstruction after the study.

At the present time reconstruction is accomplished in two steps:

First, a complete set of correlation coefficients is calculated and stored:

$$Q_{ijk\ell} \sum_{\nu=1}^{121} C_{ij}^{\nu} \, (T_{k\ell}^{\nu} - m) \quad . \qquad (10)$$

Second, the desired slice through the image is constructed;

$$I_{xyz} = \sum_{ijk\ell} \alpha_{ijk\ell}^{xyz} \, Q_{ijk\ell} \qquad (11)$$

This approach has the advantage that once the Q's are calculated any tomographic slice through the image may be rapidly constructed. However, if one or two pre-selected slices are to be reconstructed it is more rapid to calculate the appropriate spatial integrals first and sum them over the realizations.

A. Preliminary Results

Preliminary results have been obtained using computer generated data for a point source at A=B=4 cm. The data simulates the case for the aperture code shown on the lead plate in Figure 10 and described above. The first four realizations are pictured in Figure 11.

Figure 12 shows reconstructions of the point source in 3 different planes: 12-a: in-focus (A=B=4), 12-b: A=2, B=4, and 12-c: A=8, B=4. Both a central profile and an intensity modulated plan view of the reconstructed source distribution are shown. The intensity is scaled in each case such that the peak counts in the image are displayed at maximum intensity. (The small black regions result from an error in the display program.) The

low-level pattern evident in the out-of-focus reconstructions is most probably a round-off error in the present reconstruction program.

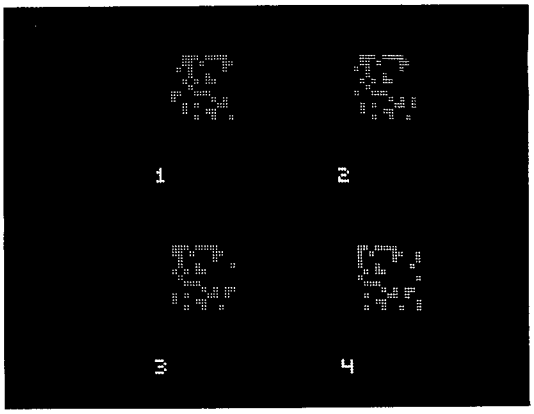

Figure 11. Simulated data for a point source located 4 cm from aperture plate shown in Figure 10. The first four realizations are shown.

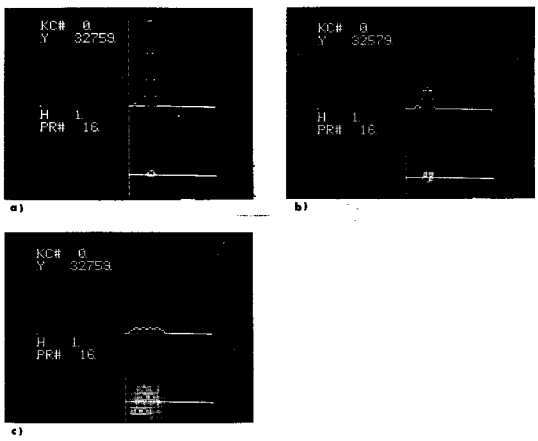

Figure 12. Profile and intensity modulated plan views of reconstructed point source for 3 different planes: a) in-focus A=4, B=4, b) A=2, B=4, c) A=8, B=4.

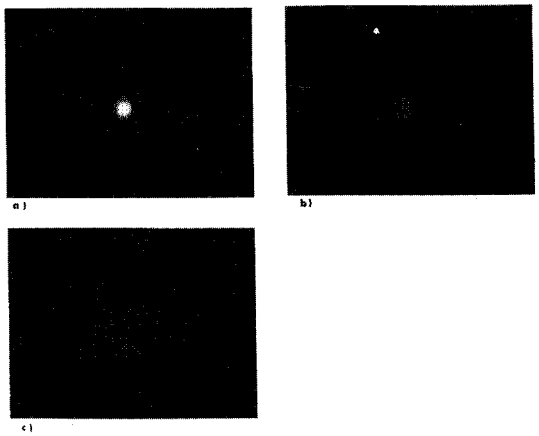

Figure 13. Plan views of same point source reconstructions pictured in Figure 12 with intensity normalized to that of in-focus peak.

The same 3 images are shown in Figure 13 with the intensity scaled to the peak of the in-focus source in order to indicate the contribution one would actually observe from an out-of-focus point source.

B. Limitations

There are two difficulties encountered in the actual application of time modulated apertures to Nuclear Medicine. The first is that the method can be applied to fast dynamic studies only with difficulty since the framing rate will have to be 121 times faster than with a stationary aperture. Data storage problems might well be encountered as a dynamic study can easily require over a hundred images. Short codes could be employed with a reduction in efficiency, or perhaps codes can be employed which will combine some of the required temporal and spatial characteristics with the aim of reducing the number of realizations needed.

angle efficiency than a pinhole for equal spatial resolution. The zone plate, for instance, has 50% open area and can yield two-to-three orders of magnitude greater collection efficiency than a pinhole of equal resolution.

This gain in solid angle provides a gain over detector noise proportional to the square root of the solid angle increase. This fact has made it possible to use x-ray film as a low cost detector despite the fog level and the small number of grains developed per interacting γ-ray (Ref. 7). The lower interaction efficiency of the film detector may be compensated in part by using large area multiple detectors for simultaneously recording several views. One can also, as a consequence of the large collection efficiency, consider large diameter, efficient photocathode devices with correspondingly high thermal noise components as a means for increasing the spatial resolution of γ-ray detectors.

It was hoped that similar gains might also be made with respect to photon noise, but it turns out than when the noise arises from statistical fluctuations in signal, the actual gain in image signal-to-noise depends explicitly on the source distribution. A detailed analysis has been performed by Barrett (Ref. 8) in the case of the zone plate and by Akcasu, May and Knoll (Ref. 9, 10, 11) in the case of the stochastic aperture. This dependence upon source distribution may be broadly characterized thus: Sizeable gains can be realized for small isolated sources and for strong sources at the expense of increased noise in the less intense regions of the image. There are a number of Nuclear Medicine imaging situations in which the detector area is poorly utilized resulting in low average count rates over the field of view. These situations should benefit markedly from coded apertures. Among these are the imaging of small organs such as the thyroid, adrenals, pancreas, kidneys and eye. Skeletal imaging, in which the sources are essentially line sources separated by empty areas, should also benefit. Some blood flow studies may also show improved signal to noise. In addition, it is possible to optimize the aperture for a given source distribution and this aspect will be discussed later.

Since coded apertures spread the information from each point in the source over a large region of the detector, non-uniformities in the detector do not as seriously degrade the image as in the case of direct imaging. Since coded apertures subtend a finite angle at a source point, the scale of the coded images contains information about the longitudinal source distribution, and the images may be reconstructed in tomographic slices corresponding to various depths in the source distribution. These properties of coded apertures provide significant motivation for their study and application to Nuclear Medicine.

The zone plate aperture has met with considerable success in both phantom imaging and clinical imaging and has yielded high quality, high resolution images (Ref. 12). There are, nevertheless, several reasons to explore alternative techniques:

In order to eliminate the conjugate and higher order images encountered with on-axis zone plates an off-axis zone plate must be employed (Ref. 1, 4). This change requires a threefold increase in the detector resolution required for a given image resolution and also requires that the source be spatially modulated by a half-tone screen with a corresponding 50% loss in efficiency.

The point response function for a finite zone plate contains residual side-lobes which can contribute artifacts to the images. Furthermore, sources out of the focal plane do not blur smoothly, but instead contribute false structure to the image. Such artifacts cannot be tolerated in clinical images. Source regions which do not project the entire zone plate onto the detector are imaged with a frequency response which depends upon position. These difficulties can all be resolved by employing time modulated apertures.

II. Time Modulated Apertures

Consider the geometry illustrated in Figure 1. Suppose that the measurement time is partitioned into M segments, and during each such interval, ν=1. . .M, a different aperture plate is inserted between the source and detector. Such a procedure is apparently a generalization of the tradi-

CODED APERTURE GAMMA-RAY IMAGING WITH STOCHASTIC APERTURES

A.Z. Akcasu[†], R.S. May[†], G.F. Knoll[†,*], W.L. Rogers[*], K.F. Koral[*], L.W. Jones[‡]

The University of Michigan

I. Introduction

A. Nuclear Medicine Imaging

Tracer doses of γ-emitting, radio-labeled pharmaceuticals have been used for a number of years for tumor localization and to provide the clinician with regional information concerning organ function and blood flow. An image of the radio-pharmaceutical distribution is formed by means of the emitted γ-rays. Elevated or depressed concentration of the tracer agent as reflected by hot or cold spots in the image is indicative of abnormalities. The γ-rays, which must be of sufficient energy to penetrate tissue with minimum scattering and absorption, cannot be refracted or reflected so the image must be formed by aperture limitation; (i.e. a pinhole in lead or multi-channel collimators). Such an aperture is extremely inefficient with solid angle efficiencies on the order of 10^{-4}; efficiency may be increased but only at the sacrifice of resolution or field of view. This, coupled with the need to minimize the radiation dose to the patient and to maintain reasonably short imaging times, results in low resolution images corrupted by noise arising from the statistical fluctuation of the γ-photon emission. A typical 25 cm diameter image field seldom contains more than 1000 resolved image elements and the information is often carried by fewer than 100,000 photons.

The penetrating nature of γ-rays combined with the need for maximum detection efficiency places severe requirements on the detector as well as the aperture. Most detectors used in Nuclear Medicine use $\frac{1}{2}$" to $1\frac{1}{2}$" thick sodium iodide scintillator as the detecting medium. A variety of schemes exist to obtain position information from these detectors with accuracy ranging between five and ten millimeters.

B. Coded Apertures

In an attempt to relieve some of the restrictions placed upon both aperture and detector a number of investigators (Ref. 1-6) have been exploring the use of stationary coded apertures for γ-ray imaging. In this paper we shall discuss the concept and application of time varying apertures to γ-ray imaging and make some comparisons to fixed apertures, in particular the zone plate, which has received the most attention to date. In the zone plate scheme a large scale zone plate made of a high atomic number material such as lead or gold is interposed between the source distribution and detector in place of the pinhole. A point source casts a geometric shadow of the zone plate onto the detector rather than being directly imaged as with a pinhole. The image of the source may be readily reconstructed optically from a reduced transparency of the zone plate shadow; alternatively if the data is available in digital form, a computer using fast transform techniques may be employed.

There are a number of reasons for investigating coded apertures and their applications in Nuclear Medicine. The intense initial interest was stimulated by the fact that a coded aperture may have a much greater solid

[†]Department of Nuclear Engineering
[*]Division of Nuclear Medicine
[‡]Department of Physics

The second limitation is that of computing time. To generate the full set of correlation coefficients for a 46 element by 46 element detector matrix and a 121 element code requires 2 hrs. and 17 min. on a NOVA-800 computer using programmed multiply-divide and 24k of core storage. Reconstruction of a 31 x 31 image slice requires about 10 minutes. Use of hard wired multiply-divide is expected to reduce these times by a factor of 5 or 10. This limitation is expected to further yield to improved reconstruction algorithims and is not at present viewed as a basic limitation.

IV. Summary

Time modulated coded apertures yield good 3 dimensional response functions, do not require half tone screens or excessive detector resolution. There are many codes available which should permit aperture optimization for many imaging situations encountered in Nuclear Medicine.

Acknowledgements

This work was supported by the National Institutes of Health Grant No. GM 16188-04 and a grant No. 474 from the Michigan Memorial-Phoenix Project. We also wish to acknowledge the computing facilities and assistance provided by Medical Data Systems for processing the coded images.

References

1. Barrett HH: Fresnel Zone Plate Imaging in Nuclear Medicine. J. Nuc. Med. 13: 382, 1972.

2. Rogers WL, Han KS, Jones LW, Beierwaltes WH: Application of a Fresnel Zone Plate to Gamma-Ray Imaging. J. Nuc. Med. 13: 612, 1972.

3. Dicke RH: Scatter-Hole Cameras for X-rays and Gamma-Rays. Astrophysical J. 153: L101, 1968.

4. Rogers WL, Jones LW, Beierwaltes WH: Imaging in Nuclear Medicine with Incoherent Holography. Optical Engineering 12: 13, 1973.

5. Barrett HH, Wilson DT, DeMeester GD: "The Use of Half-tone Screens in Fresnel Zone Plate Imaging of Incoherent Sources." Opt. Comm. 5: 398, 1972.

6. Walton PW: An Aperture Imaging System with Instant Decoding and Tomographic Capabilities. J. Nuc. Med. 14: 861, 1973.

7. Barrett HH, DeMeester GD, Wilson DT, Farmelant MH: Recent Advances in Fresnel Zone Plate Imaging, Medical Radioisotope Scintigraphy, 1972, Vol. I. 282-283. IAEA, Vienna (1973).

8. Barrett HH, DeMeester GD: "Quantum Noise in Fresnel Zone Plate Imaging. Raytheon Technical Report T-972, 1973.

9. May RS, Akcasu AZ, Knoll GF: γ-Ray Imaging With Stochastic Apertures. (Submitted to Applied Optics.)

10. May RS: Stochastic Aperture Techniques in Gamma Ray Image Formation. Ph.D. Thesis, The University of Michigan, (1974).

11. May RS, Knoll GF, Akcasu AZ: A Cross-Correlative Technique for Gamma-Ray Imaging. (Submitted to J. Nuc. Med., Nov. 1973).

12. Farmelant MH: Improved Anatomical Definition by a Fresnel Zone Plate Imager. (Abstract) J. Nuc. Med. 14: 393, (1973).

13. Hossfeld F, Amadori R: On Pseudorandom and Markov Sequences Optimizing Correlation Time-Of-Flight Spectrometry. Kernforschungsanlage Julich Report, Jul-684-FF: (1970).

14. Rydin RA, Hooper RJ: Numerical Evaluation of Spatially Dependent Dynamic Reactor Systems Using Pseudorandom Signals. Nuc. Sci. Eng. 38: 216-228, (1969).